ACCOUNTS of chemical research

Article

Cite This: Acc. Chem. Res. XXXX, XXX, XXX-XXX

pubs.acs.org/accounts

Coherence Spectroscopy in the Condensed Phase: Insights into Molecular Structure, Environment, and Interactions

Jacob C. Dean*,†,‡ and Gregory D. Scholes*,†

†Department of Chemistry, Princeton University, Princeton, New Jersey 08544, United States

‡Department of Physical Science, Southern Utah University, Cedar City, Utah 84720, United States

CONSPECTUS: The role of coherences, or coherently excited superposition states, in complex condensed-phase systems has been the topic of intense interest and debate for a number of years. In many cases, coherences have been utilized as spectators of ultrafast dynamics or for identifying couplings between electronic states. In rare cases, they have been found to drive excited state dynamics directly. Interestingly though, the utilization of coherences as a tool for high-detail vibronic spectroscopy has largely been overlooked until recently, despite their encoding of key information regarding molecular structure, electronically sensitive vibrational modes, and intermolecular interactions. Furthermore, their detection in the time domain makes for a highly comprehensive spectroscopic technique wherein the phase and dephasing times are extracted in addition to amplitude and intensity, an element not afforded in analogous frequency domain "steady-state" measurements. However, practical limitations arise in disentangling the large number of coherent signals typically accessed in broadband nonlinear spectroscopic experiments, often complicating assignment of the origin and type of coherences generated.

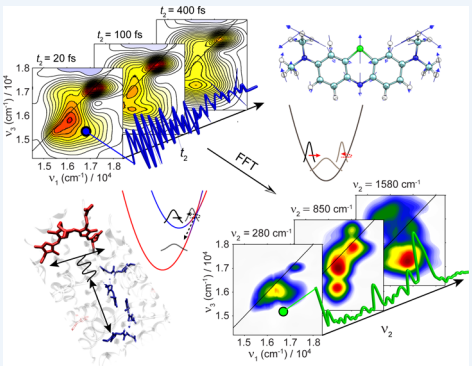

Two-dimensional electronic spectroscopy (2DES) affords an avenue by which to disperse and decompose the large number of coherent signals generated in nonlinear experiments, facilitating the assignment of various types of quantum coherences. 2DES takes advantage of the broad bandwidth necessary for achieving the high time resolution desired for ultrafast dynamics and coherence generation by resolving the excitation axis to detect all excitation channels independently. This feature is beneficial for following population dynamics such as electronic energy transfer, and 2DES has become the choice method for such studies. Simultaneously, coherences arise as oscillations at well-defined coordinates across the 2D map often atop those evolving population signals. By isolating the coherent contribution to the 2DES data and Fourier transforming along the population time, a 3D spectral representation of the coherent 2D data is generated, and coherences are then ordered by their oscillation frequency, ν_2. Individual coherences can then be selected by their frequency and evaluated via their distinct "2D coherence" spectra, yielding a significantly more distinctive set of spectroscopic signatures over other 1D methodologies and single-point 2DES analysis. Given that coherences of different origin result in unique 2D coherence spectra, these characteristics can be catalogued and compared directly against experiment for prompt assignment, a strategy not afforded by traditional 2DES analysis.

In this Account, a structure-driven time-independent spectral model is discussed and employed to compare the 2D fingerprints of various coherences to experimental 2D coherence spectra. The frequency-domain approach can easily integrate *ab initio* derived vibronic parameters, and its correspondence with experimental coherence spectra of a model compound is demonstrated. Several examples and applications are discussed herein, from 2D Franck−Condon analysis of a model compound, to identifying the signatures of interpigment vibronic coupling in a photosynthetic light-harvesting complex. The 3D spectral approach to 2DES provides remarkable spectroscopic detail, in turn leading to new insights in molecular structure and interactions, which complement the time-resolved dynamics simultaneously recorded. The approach presented herein has the potential to distill down the convoluted set of nonlinear signals appearing in 2D coherent spectra, making the technique more amenable to high-detail vibronic spectroscopy in inherently complex condensed phase systems.

I. INTRODUCTION

Time-dependent quantum mechanics provides a holistic description of a molecule's structure and dynamics over all degrees of freedom and can generally be related back to our familiar time-independent view by a simple Fourier transform.[1,2] In the same way, time-resolved coherent spectroscopy is a comprehensive method for spectroscopy and dynamics. It provides time-domain information in the form of photoinitiated dynamics with a resolution down to femtoseconds, while simultaneously revealing a molecule's frequency-domain spectroscopic content at a level of detail rarely realized by steady-state methodologies. The latter feature comes in the form of coherences, or wavepackets, whose time evolution

Received: July 25, 2017

ACS Publications © XXXX American Chemical Society

DOI: 10.1021/acs.accounts.7b00369
Acc. Chem. Res. XXXX, XXX, XXX−XXX

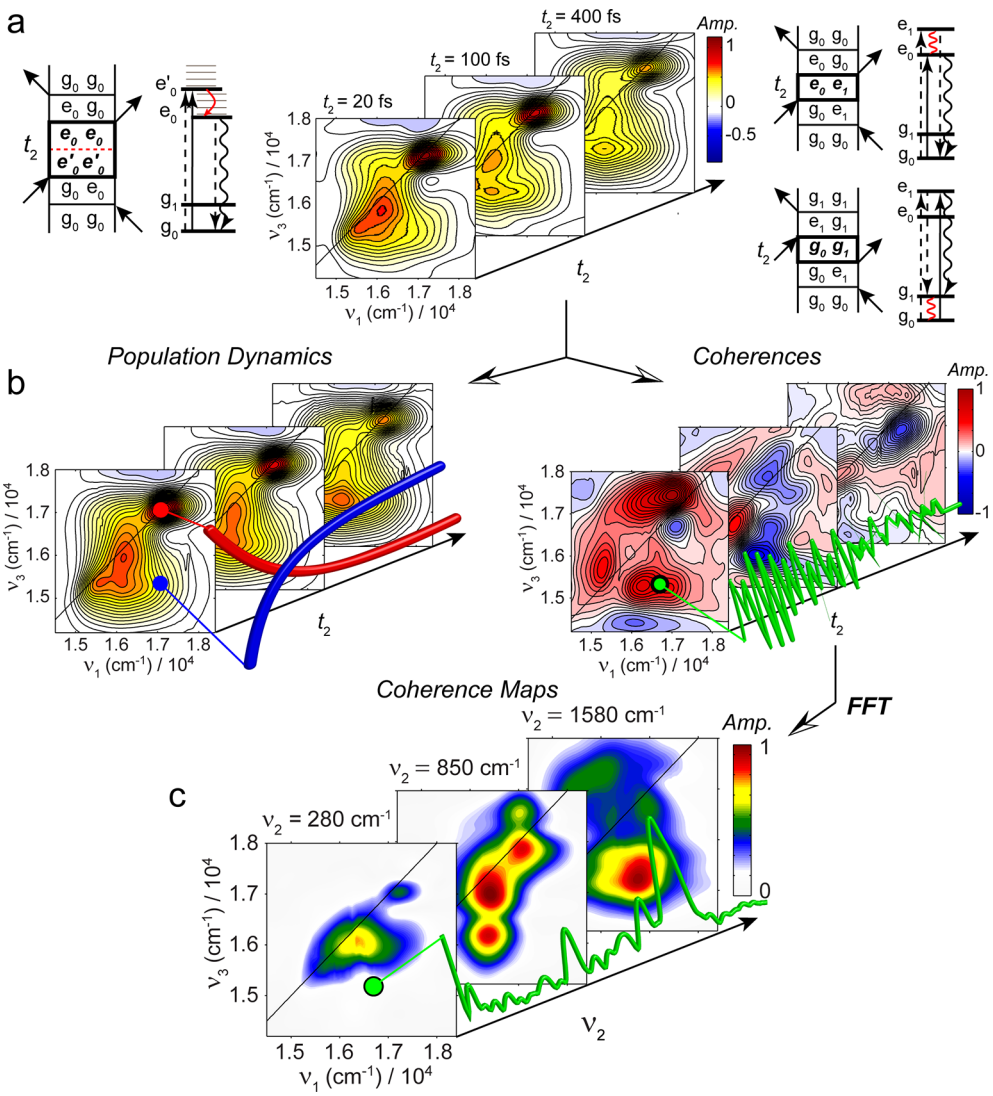

Figure 1. (a) Representation of 2DES data and example double-sided Feynman diagrams for population transfer (left) and coherence generation (right). (b) The 2DES data is composed of population and coherent dynamics during the population time, t_2, and can be separated. (c) Fourier transformation of the coherence data along t_2 results in a set of 2D coherence spectra separated by their oscillation frequency, ν_2.

maps out the complex multidimensional potential energy surfaces of the molecule.

Coherent multidimensional spectroscopy has been a method of choice for ultrafast dynamics because ultrashort pulses required to attain femtosecond time resolution are broadband. While a broadband pump pulse generally complicates the analysis of dynamics in transient absorption due to the native uncertainty in excitation frequency, in two-dimensional spectroscopy, the excitation axis is recovered, thereby casting the multitude of generated nonlinear signals into frequency−frequency correlation maps of the excitation, ν_1, and third-order signal emission frequencies, ν_3. In this way, all signals originating from separate excitations induced by the broadband pulses are dispersed and can be followed independently allowing for simultaneously high time and frequency resolution. The broadband pulses that permit such high time-resolution also lead to coherent excitation of multiple quantum states simultaneously, that is, superposition states, in the ground and excited electronic manifolds of the chromophore. These "coherences" are born in a local region of the molecular potential, then traverse the surface introducing "beats", or oscillations in the recorded nonlinear signal. These beats occur at frequencies matching the energy splittings between those coherently excited eigenstates. Taken together with the amplitude, phase, and dephasing time information recovered through such time-domain measurements, "coherence spectroscopy" reveals the full coherent evolution of the system and retrieves its vibronic spectrum when Fourier transformed (FT) into the frequency domain.[1,3−6] Coherent multidimensional spectroscopy is therefore implicitly sensitive to molecular structure.

Generally, any set of quantum states coupled through a common state can be coherently excited. For excitonic systems with strongly coupled sites, an electronic/excitonic coherent superposition of states can be excited, but they dephase quickly on time scales of ∼100 fs, similar to optical coherence between ground and excited states during time period t_1.[7] Vibrational coherence can occur in either the ground or excited electronic state, and it can evolve for picoseconds or longer. In electronic spectroscopy, only those vibrations that are activated upon electronic excitation, that is, those coordinates that are displaced between electronic states, will give rise to vibrational

DOI: 10.1021/acs.accounts.7b00369
Acc. Chem. Res. XXXX, XXX, XXX−XXX

coherence. This feature is advantageous for evaluating vibrational coherence in complex systems such as light-harvesting complexes, where the electronic chromophore selectivity distills down an intractable number of vibrational modes to only those that are sensitive to electronic excitation. In special circumstances where the vibrational and electronic degrees of freedom are no longer separable (breakdown of the Born−Oppenheimer approximation), mixed vibrational−electronic, or "vibronic", coherence can also occur.[8−13] Understanding the signatures of all of these types of coherence is paramount to utilizing them as a spectroscopic tool for uncovering critical, and otherwise hidden, insights associated with molecular structure.

In this Account, a simple semiquantitative approach based entirely in the frequency domain is discussed for assigning and interpreting coherences generated in coherent spectroscopic experiments. An example is given for the photodynamic therapy (PDT) chromophore methylene blue, where detailed vibronic analysis is achieved to yield the 2D signatures of vibrational fundamentals, overtones, and combination coherences. Further, we demonstrate the use of electronic chromophores as probes of local protein structure in pigment−protein complexes. Lastly, the signatures of interpigment vibronic interactions are explored in the phycobiliprotein PC645 via 2D coherence analysis.

II. TWO-DIMENSIONAL ELECTRONIC SPECTROSCOPY AND 2D COHERENCE MAPS

Broadband transient absorption (BBTA) is an effective tool to characterize the population dynamics of the system under study as well as provide an overview of the coherences generated. While fundamentally 2DES contains all of the information found in BBTA measurements, in practice the fast acquisition times and ease of sampling in BBTA lends complementarity to a joint approach. Details regarding the BBTA/2DES experiments and data acquisition can be found elsewhere;[14−16] here we only discuss those points most relevant to coherence spectroscopy. The set of nonlinear signals generated from ultrafast pulses can be categorized as either *populations* or *coherences* depending on whether a population state or coherence is generated by the pump pulse sequence, and it evolves during the population time period, t_2. Examples are given on the left and right branches of Figure 1 respectively.[14,16]

Population pathways are most commonly the features of interest in TA as they carry the information related to dynamics following photoexcitation (Figure 1b). An example is electronic energy transfer in which ground state bleach (GSB) and stimulated emission (SE) spectral signals of a donor chromophore evolve into the corresponding signals of the acceptor (Figure 1a left). 2DES conveniently illuminates these pathways as below-diagonal cross-peaks, where the initially excited donor absorbs light at ν_1, then transfers energy downhill to the acceptor, whose photoexcitation is detected in ν_3. The population dynamics can be modeled with a multiexponential fitting procedure and then subsequently removed from the data leaving behind only coherent signals (Figure 1b, right). In order to generate coherences, the pump pulse duration must be shorter than the vibrational period, and the bandwidth must span all quantum states in the superposition. Fourier transformation of the signal-amplitude modulations along t_2 leads to a nonlinear "vibronic" spectrum, with a frequency resolution that depends only on the dephasing time of the coherence, oftentimes leading to line widths of approximately 10−20 cm^{-1}. In 2DES, an FT can be performed along t_2 at each (ν_1,ν_3) point to yield a three-dimensional spectrum, (ν_1,ν_2,ν_3), best visualized as 2D maps of particular ν_2 slices (Figure 1c).

Even for the simplest 4-level vibronic system, however, a total of 16 possible pathways, or nonlinear signals, are associated with vibrational coherence (excluding excited state absorption signals). This is exemplified in Figure 2a, which

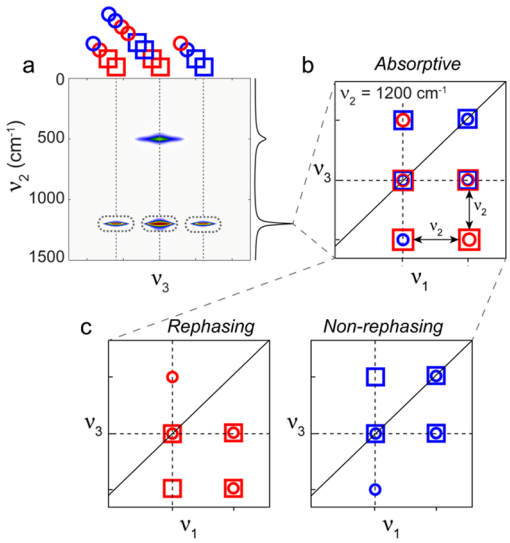

Figure 2. Decomposition of coherent signals from (a) BBTA to (b) absorptive 2D coherence map, and (c) its constituent rephasing and non-rephasing spectra. Squares represent GSB signals, and circles represent SE.

shows significant pile-up of coherent signals (squares = GSB and circles = SE) in an example BBTA FT spectrum, precluding determination of the coherence character or origin. The 2D analog to Figure 2a is the absorptive 3D spectrum, which disperses the signals for each ν_2 over the excitation axis dividing each "stack" of signals in BBTA by two (Figure 2b). Furthermore, in traditional 2DES implementations, the rephasing (red) and non-rephasing (blue) spectra, which sum together to form the absorptive spectrum, are recorded independently separating those signal pathways, thereby splitting the absorptive signals into another two halves, each with their own unique spectral patterns (Figure 2c). This decomposition enables a joint rephasing/non-rephasing spectral analysis since coherences of various character imprint uniquely on each; additionally, single unique signals can finally be isolated. Recognizing the distinctive amplitude patterns illuminated in rephasing and non-rephasing coherence spectra then gives rise to a thorough fingerprinting mechanism for coherence assignments, where such detail is generally concealed in BBTA.

III. TOWARD DETAILED VIBRONIC SPECTROSCOPY IN THE CONDENSED PHASE: FRANCK−CONDON COHERENCE ANALYSIS OF METHYLENE BLUE

Each nonlinear signal (squares or circles, Figure 2) can be represented in the form of double-sided Feynman diagrams (Figure 1a), which represent a form of book-keeping for the four light−matter interactions leading to signal generation, and their spectral coordinates in 2DES maps are naturally encoded therein. The amplitude of each signal can be represented most simply in the "stick spectrum" limit,[17] where the individual

DOI: 10.1021/acs.accounts.7b00369
Acc. Chem. Res. XXXX, XXX, XXX−XXX

time-independent transition dipole moments, μ, of each field−matter interaction leading to that signal are multiplied together yielding a product of four terms, $\mu^{(1)}\mu^{(2)}\mu^{(3)}\mu^{(4)}$. In a vibronic system, each μ is determined by the electronic absorption strength scaled by individual vibrational overlap integrals between the ground and excited state vibrational levels accessed. Therefore, for a single excited electronic state each interaction can be represented by the modulus of the vibrational amplitude alone, that is, $\mu_{v'v''} = |\langle\chi_{v'}|\chi_{v''}\rangle| = \sqrt{\text{FCF}}$, where v′ and v″ are the excited and ground state vibrational quanta, χ_v are the associated vibrational wave functions, and FCF stands for the Franck−Condon factor.

The benefit of representing these nonlinear signals in such a time-independent format is that the parameters are implicitly derived from the time-independent Hamiltonian and can be computed *ab initio*. In other words, the model is truly atomistic, structurally driven, and simple. The Franck−Condon factors for all possible vibronic transitions are calculated using the displacements in equilibrium geometry and vibrational frequencies (which can be obtained by standard calculations in a modern quantum chemistry package) and those parameters can be input into a simulation that maps out all signal pathways leading to coherences across the 2D (ν_1,ν_3) map oscillating at ν_2. Therefore, the frequency-domain representation of the nonlinear spectroscopy experiment (ν_1,ν_2,ν_3) can be compared directly. Upon doing so, unique signatures are obtained for ground and excited state fundamental vibrational coherences, overtone and combination coherences, and electronic and "vibronic" coherences.

While simple and easily comparable against 2D coherence maps, several assumptions and shortcomings of the model must be noted when evaluating data, and they are discussed in detail elsewhere.[18,19] Namely, the approach is devoid of line shape information, it assumes identical decoherence times for all coherences, and the laser excitation spectrum is not explicitly incorporated, assuming equal intensity across all frequencies. Nevertheless, the predominant advantage of this approach is the simplification of the coherence assignment process to simple pattern recognition in 2D coherence maps, since each type of coherence carries particular 2D signatures. Additionally, the determination of vibronic parameters *ab initio* relinquishes the reliance on spectral fitting of steady-state spectra which obscures entirely those vibronic characteristics often driving dynamics in subsequent simulations. In fact, the advantages of exhaustive quantum dynamics approaches, such as the numerically exact hierarchical equations of motion (HEOM) method, are often offset by the reliance on limiting approximations and highly approximated spectral densities to curb its high computational cost.

Here, we carry out a detailed vibronic analysis of the visible absorption band of methylene blue (MB) utilizing this approach in tandem with BBTA/2DES.[19] MB is a cationic dye (Figure 3a) used most recently in photodynamic therapy due to its large electronic absorption in the therapeutic window of the skin and its high quantum yield for forming singlet oxygen *in vivo*.[20] Despite widespread use of these photochemical properties, little is known about the nature of the involved excited states. Figure 3a shows the absorption (black) and fluorescence spectra (red) of MB along with the pulse spectrum (blue) used for ultrafast measurements. The BBTA spectrum in Figure 3b reveals oscillations superimposed on the evolving GSB/SE population signals peaking between the absorption and fluorescence maxima near 15000 cm^{-1}. Isolation

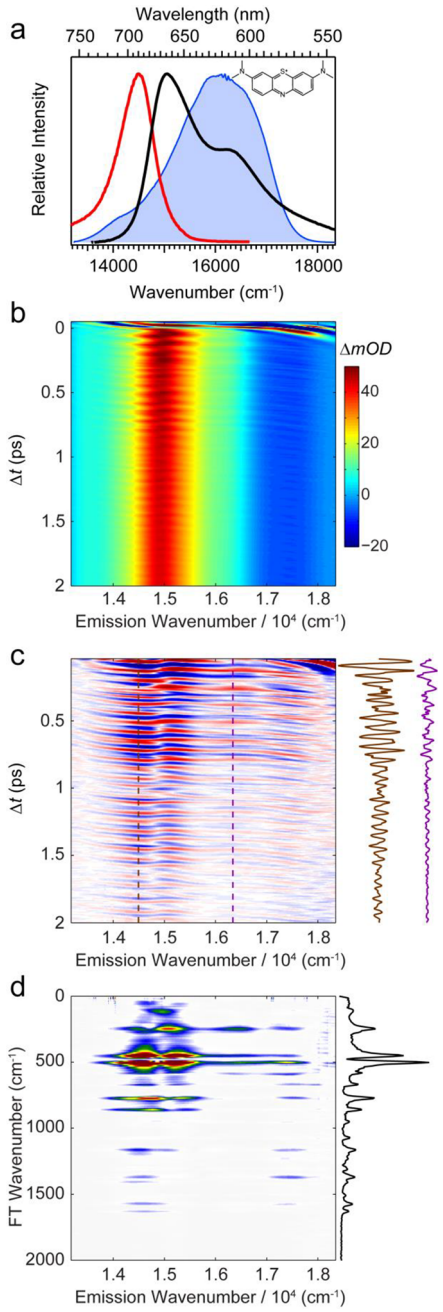

Figure 3. (a) Absorption (black) and fluorescence (red) spectra of methylene blue, and the pulse spectrum employed for BBTA/2DES measurements (blue). (b) Parallel-polarized BBTA spectrum of MB. (c) Coherent BBTA spectrum and (d) its Fourier transform spectrum. Adapted with permission from ref 19. Copyright 2015 ACS.

of those coherences in Figure 3c illuminates a node shifting to the red as the population undergoes a dynamic Stokes shift over ∼2 ps. The FT spectrum (Figure 3d) reveals a vibrational spectrum resolved across all probe wavelengths, and again the node is found very near the absorption maximum signaling a predominance of ground state coherences.[4,21] The largest amplitude is found at 450 and 500 cm^{-1}, and the spectrum integrated over the GSB/SE region is shown to the right of Figure 3d.

Density functional theory (DFT) calculations show that MB is C_{2v} symmetric in the ground state with 108 normal modes. The DFT Franck−Condon (FC) simulation is shown in Figure

DOI: 10.1021/acs.accounts.7b00369
Acc. Chem. Res. XXXX, XXX, XXX−XXX

4a with all transitions labeled according to the Mulliken scheme. Some of those modes are given in Figure 4b. The

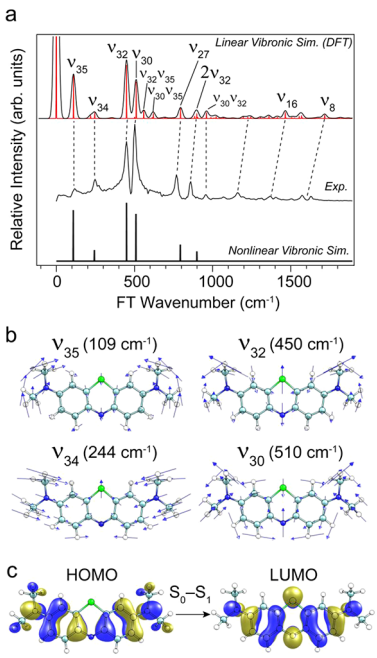

Figure 4. (a) DFT calculated linear Franck−Condon simulation (top), experimental integrated FT spectrum (middle), and nonlinear Franck−Condon simulation (bottom). (b) Vibronically active modes assigned in FT spectrum. (c) Frontier orbitals for S_0−S_1 transition. All calculations were performed at the M05-2X/6-311+G(d,p) level of theory. Adapted with permission from ref 19. Copyright 2015 ACS.

GSB/SE integrated FT spectrum is shown below for comparison, and the DFT simulation captures the activated vibrational coherences and their frequencies remarkably well. The agreement can be used to assign all of the recorded coherences to specific modes and the number of quanta involved in each. Modes involving motion of the central CSC/CNC ring and peripheral $CN(CH_3)_2$ groups dominate the vibronic activity and can be rationalized based on differences in bond order between S_0 and S_1 (Figure 4c).

As anticipated, most of the coherences are assigned to fundamentals ($\Delta\nu = 1$); however, the simulation enables us to pinpoint at least one overtone of the large ν_{32} CSC/CNC bending mode and the $\nu_{30}\nu_{32}$ combination coherence in the experiment. The agreement between the linear FC model and nonlinear experiment suggests that summing over all coherent pathways leads to a relatively unbiased scaling of the transition dipole terms in all possible $\mu^{(1)}\mu^{(2)}\mu^{(3)}\mu^{(4)}$ products. For comparison, the FC factors from the linear model were used to compute directly the integrated nonlinear spectrum for the largest few modes (Figure 4a, bottom). Each stick was calculated by summing the amplitudes of all possible GSB and SE Feynman pathways:[19]

$$A = \sum_n (\mu^{(1)}\mu^{(2)}\mu^{(3)}\mu^{(4)})_n \tag{1}$$

$$A_{\mathrm{Fund}}^{\mathrm{GSB}} = 2\mu_{10}{}^2(\mu_{00}{}^2 + \mu_{11}{}^2 + 2\mu_{00}\mu_{11}) \tag{2a}$$

$$A_{\mathrm{Fund}}^{\mathrm{SE}} = 2\mu_{10}{}^2(2\mu_{00}{}^2 + 2\mu_{00}\mu_{11}) \tag{2b}$$

$$A_{\mathrm{OT}}^{\mathrm{GSB}} = 2\mu_{10}\mu_{21}(2\mu_{00}\mu_{20} + 2\mu_{20}\mu_{22} + \mu_{10}\mu_{21}) \tag{3a}$$

$$A_{\mathrm{OT}}^{\mathrm{SE}} = 4\mu_{00}\mu_{10}\mu_{20}\mu_{21} \tag{3b}$$

The results indeed closely resemble the linear model suggesting that even a cursory linear FC model is a good approximation for the total nonlinear coherence spectrum.

Figure 5a shows representative absorptive 2D spectra displaying the evolution of the coherence in t_2. The square

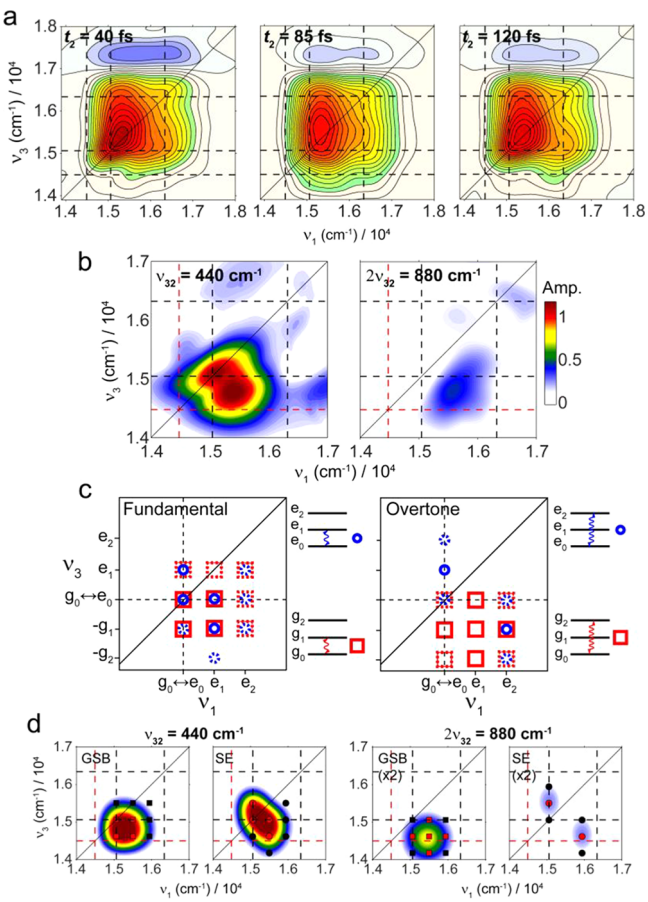

Figure 5. (a) Absorptive 2D spectra of MB showing wavepacket evolution. (b) 2D rephasing coherence maps of ν_{32}. (c) Schematics of rephasing 2D coherence maps for fundamental (left) and overtone coherences (right) with the respective energy-level diagrams to right. Red squares indicate GSB pathways and blue circles indicate SE; dashed symbols yield negligibly small amplitudes. (d) Simulated Franck−Condon coherence maps for each coherence demonstrating the variation in 2D fingerprints of each type. Adapted with permission from ref 19. Copyright 2015 ACS.

shape of the positive signal amplitude can be related to the absorption spectrum, which features a broad origin and vibronic shoulder. The rephasing 2D coherence maps for ν_{32} and its overtone coherence are shown in Figure 5b following the extraction procedure discussed in section II. Figure 5c displays the 2D patterns expected after mapping out all GSB (squares) and SE (circles) pathways for the six-level model shown. Solid squares and circles indicate the four signals contributing the largest amplitude to the 2D map, and their dashed counterparts arise at significantly lower amplitude due to interactions with $\nu = 2$ states. For ground state coherence, we expect most of the amplitude to be localized in a box below the diagonal, while SE

DOI: 10.1021/acs.accounts.7b00369
Acc. Chem. Res. XXXX, XXX, XXX−XXX

shows a unique excited state signal above the diagonal. As indicated in the schematic, the splitting between each neighboring signal is the respective ν_2 frequency. Using the vibrational overlap integrals taken from the DFT FC simulation, we can simulate the 2D coherence maps for ground and excited state coherence (Figure 5d). As expected from BBTA results, the ν_{32} amplitude is almost exclusively of ground state origin showing maximal amplitude at the center of the four GSB signals (due to spectral broadening).

While the signals for fundamentals are all separated by ν_2 in the ν_1/ν_3 directions, overtone coherences yield their own very unique signatures. Based on the schematic in Figure 5c (right), GSB signals are all separated by the fundamental frequency, that is, $1/2\nu_2$, with an amplitude pattern that makes a cross with the centermost point $(\nu_1, \nu_3) = (+1/2\nu_2, -1/2\nu_2)$. Indeed the 2D coherence map shows the maximum amplitude at this point, unambiguously unveiling the ground state overtone character of the coherence.

IV. COHERENCE AS A PROBE OF LOCAL STRUCTURE AND ENVIRONMENT

The structural sensitivity gained by vibrational coherence evaluation paves the way for extending such analyses to complex multichromophoric systems such as photosynthetic light-harvesting complexes (LHCs). The pigments incorporated into LHCs are typically arranged in highly specific architectures defined by the protein scaffold in order to maximize light capture and energy transfer efficiency.[22−24] This results in the collective optimization of pigment spectral properties and a complex network of intermolecular interactions, which ultimately drive energy transport throughout the protein.

Phycobiliproteins uniquely incorporate linear tetrapyrrole pigments, called bilins, which are covalently attached to the apoprotein and are conformationally and spectrally flexible compared to their chlorophyll counterparts. As such, they are kept in fairly contorted geometries likely associated with a spectral tuning mechanism of the protein. Thus, the vibronic activity of the incorporated bilins will be largely defined by their protein-manipulated geometries and local protein/solvent environment. Given the role that the protein plays in steering the spectroscopic properties of its pigments, it is a natural realization that the pigments themselves can report back on their immediate environment. The pigment selectivity of electronic spectroscopy combined with the resolving power of BBTA and 2DES makes for a thorough fingerprinting mechanism then for the collection of pigments within a protein.

One example given here is the use of coherence signatures to investigate the fidelity of cooperative folding of the subunits incorporated into the PE545 light-harvesting antenna of the cryptophyte algae *Rhodomonas* CS24 (Figure 6a, inset). Phycobiliproteins produced by cryptophyte algae display a quaternary structure composed of two larger β-subunits binding three bilins each and two α-subunits each binding a single bilin. Recently, denaturation by pH treatment and subsequent separation of the α- and β-subunits enabled refolding studies when the subunits were recombined and brought back to neutral pH.[25] The reformed proteins were shown to return to their native quaternary structure by a self-chaperoning mechanism,[25] but the absolute structural fidelity of the refolded PE545 was only inferred through steady-state spectroscopy. The internal metrics granted by time- and frequency-domain coherence analysis, however, enabled the necessary structural

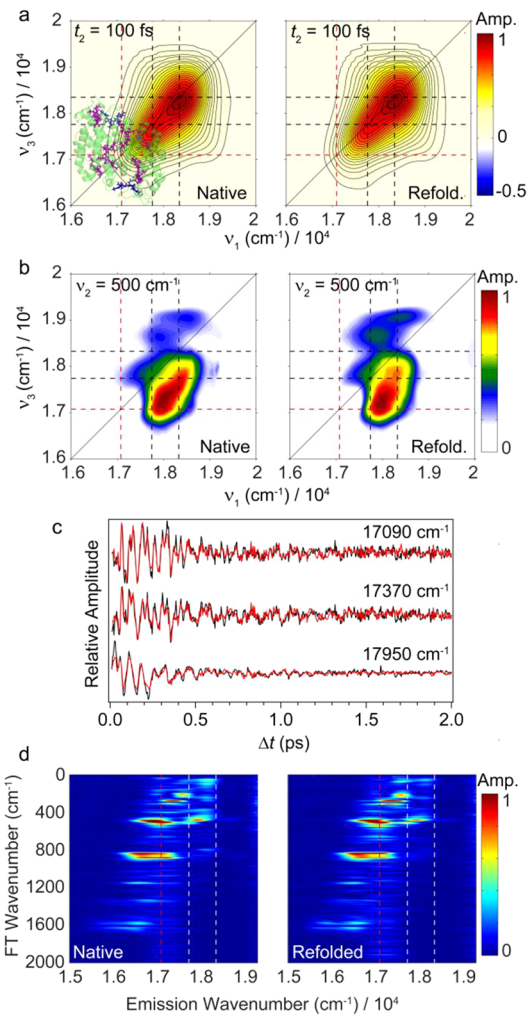

Figure 6. (a) Normalized 2D spectra for native and refolded PE545; inset shows the PE545 crystal structure. (b) 2D coherence maps at 500 cm^{-1} for native and refolded proteins. (c) BBTA traces of native (black) and refolded (red) proteins at various emission wavenumbers. (d) Fourier power spectra from coherent BBTA for native and refolded PE545. Reprinted with permission from ref 25. Copyright 2017 Wiley-VCH Verlag Gmbh & Co. KGaA, Weinheim.

sensitivity for validating the absolute reconstitution of the protein structure. Equivalent 2D spectra for both the native and refolded proteins are shown in Figure 6a, and the 2D coherence map of the strongest coherence at 500 cm^{-1} is shown below. The maps yield identical spectral features across all pigments, and the coherent time traces in BBTA demonstrate indistinguishable beating patterns in both relative amplitude and phase for the set of coherences shown in Figure 6d. The sensitivity of the vibrational coherences to protein structure was referenced by acquiring spectra for the unfolded α-subunit alone, proving considerably different than the folded protein and demonstrating the sensitivity of the bilin vibronic activity to its local environment and conformation.[25]

V. 2D COHERENCE MAPS REVEAL VIBRONIC COUPLING IN A LIGHT-HARVESTING PROTEIN

Since early reports of seemingly long-lived electronic coherence in natural light-harvesting proteins,[26,27] the identity and role of coherences in the energy transfer process has been an extensively debated topic. Many recent works involving 2DES

DOI: 10.1021/acs.accounts.7b00369
Acc. Chem. Res. XXXX, XXX, XXX−XXX

modeling suggest that vibronic coupling between donor and acceptor pigment states can explain the persisting coherent oscillations that bear resemblance to electronic delocalization.[8−10,13,28−30] To begin to address the functional potential of such "mixed" vibrational−electronic couplings, its seemingly subtle fingerprint necessitates experiments and analysis able to resolve interpigment interactions with quantum-state resolution. In other words, the state assignments and distinct spectroscopic signatures of vibronic mixing must be ascertained to first properly identify its presence and to what pigments it is acting. The markedly altered energy transfer landscape enabled by these bridging resonances elicits a more active role for pigment vibrations in delocalizing electronic excitations.[28,31−33]

Considering the larger vibronic activities and relatively weak electronic couplings of bilins compared to chlorophyll,[33] phycobiliproteins serve as candidate LHCs for examining vibronic mixing as a mechanism for energy transfer over the large distances separating bilins (∼20 Å) and the large energy gaps between them. To that end, the primary antenna protein of the cryptophyte *Chroomonas mesostigmatica* (CCMP 269), phycocyanin 645 (PC645, Figure 7b), was recently found to

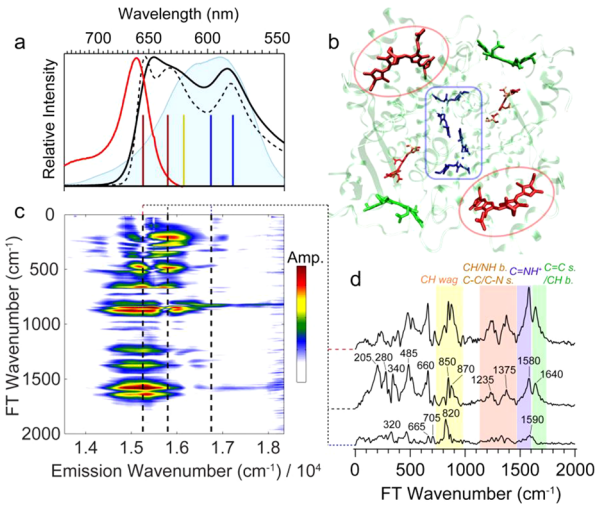

Figure 7. Spectroscopic overview of PC645.[18] (a) Absorption (black, solid) and fluorescence spectra (red) at ambient temperature and 77 K absorption spectrum (black, dashed). The pulse spectrum is shown in blue. (b) Crystal structure of PC645 with pigments color-coded according to the stick spectrum. (c,d) Fourier transform spectrum of coherent BBTA; colored regions in panel d denote the mode assignments given above. Adapted with permission from ref 18. Copyright 2016 Elsevier Inc.

exhibit such characteristics.[18] PC645 harvests the yellow-orange region of the solar spectrum (Figure 7a) lending the cryptophyte organism a complementary absorption to chlorophyll for maximal light capture in low-light conditions. PC645's functional role as the primary antenna is then to capture available light and rapidly down-convert it for ensuring a compatible transfer to chlorophyll-containing photosystems, which incorporate reaction centers. Indeed, the fastest energy transfer pathway occurs from the primary donor dihydrobiliverdin (DBV, blue) lower exciton state to the final phycocyanobilins (PCB, red) at the periphery of the complex. Therefore, direct transfer to the energy terminus of the pigment network occurs in a single rapid step, begging the question of the driving mechanism that directs such an energetically remote ($\Delta E \approx 1500$ cm^{-1}) channel.

The FT spectrum for PC645 is given in Figure 7c and displays rich vibronic structure with amplitude mostly localized in the PCB spectral region. One-dimensional traces are shown for clarity in Figure 7d. The largest amplitudes are found in the C−H bending region near 850 and the ∼1600 cm^{-1} C═N/C═C stretching region. These modes can be found extending well into the DBV region. At this point, it is noted that the high frequency C═N stretch mode matches closely the PCB−DBV energy gap.

In order to investigate the coherence spectrum in greater detail, we turn to 2DES and 2D coherence maps to fingerprint notable features in the BBTA spectrum. The 2DES spectra at both ambient temperature and 77 K reveal cross-peaks connecting the lower DBV bleach transition and PCB acceptor states already at t_2 = 0 fs signaling their coupling. These positions are marked by dashed lines in Figure 8a. As expected from BBTA, large amplitude oscillations are found in the 2D map predominantly along $\nu_3 \approx 15250$ cm^{-1}, the terminal PCB frequency. An antidiagonal slice through the DBV/PCB regions (Figure 8a) displays high frequency oscillations with a ∼21 fs period and dephasing time of ∼350 fs. Transforming the oscillatory data into spectral form, the 2D coherence maps for this frequency are shown in Figure 8b. Upon inspection, it is immediately striking that the features in both rephasing and non-rephasing spectra resemble electronic coherence,[34−36] a surprising result given the 1500 cm^{-1} separation of pigment states across the absorption spectrum and the drastically smaller electronic coupling between them. We note that several control experiments proved these features robust and unaffected by bandwidth-induced filtering effects.[18]

To investigate the amplitude patterns of the high-frequency coherence, two models were tested involving the large amplitude C═N stretch vibrations. For vibrational coherence localized on the acceptor PCBs (Figure 8c(left),d), the transition dipole prefactors defining the vibrational amplitude in the excited state should be nearly equivalent to the ground state. This is clear by comparing pure excited state and ground state features CP1 and CP3 respectively, and illustrates a characteristic vibrational fingerprint. Comparing the experimental result to the charted signals however suggests that interactions involving one quantum of the C═N stretch mode in the excited state carry significantly larger amplitude than those with the ground state mode, that is, $\mu_{10} > \mu_{01}$, and CP1/CP2 dominate the amplitude in the rephasing map (diagonal peaks are enhanced in non-rephasing). This nontrivial disparity can be explained by intensity-borrowing effects in the excited manifold facilitated by resonance of the PCB C═N mode with the PCB−DBV splitting and reveals a new set of characteristic 2D fingerprints in stark contrast to those explored in section III. To simulate the 2D coherence map for this interpigment vibronic coupling scenario, the mixed vibronic wave functions for all states were generated following diagonalization of an appropriate PCB−DBV electronic−vibrational Hamiltonian.[37] The vibronic wave functions were then used to compute the overlap integrals (amplitudes) for all transitions between them and then were input into the 2D coherence amplitude simulation. The result is shown in Figure 8e and yields features highly reminiscent of both experimental spectra, with peak amplitudes some 5-fold larger than pure vibrational coherences.[8] Within the model, an amplitude enhancement for the excited state PCB fundamental is realized through mixing with the lower DBV electronic origin, donating significant oscillator strength to the interaction (Figure 8c, right). Importantly, both

DOI: 10.1021/acs.accounts.7b00369
Acc. Chem. Res. XXXX, XXX, XXX−XXX

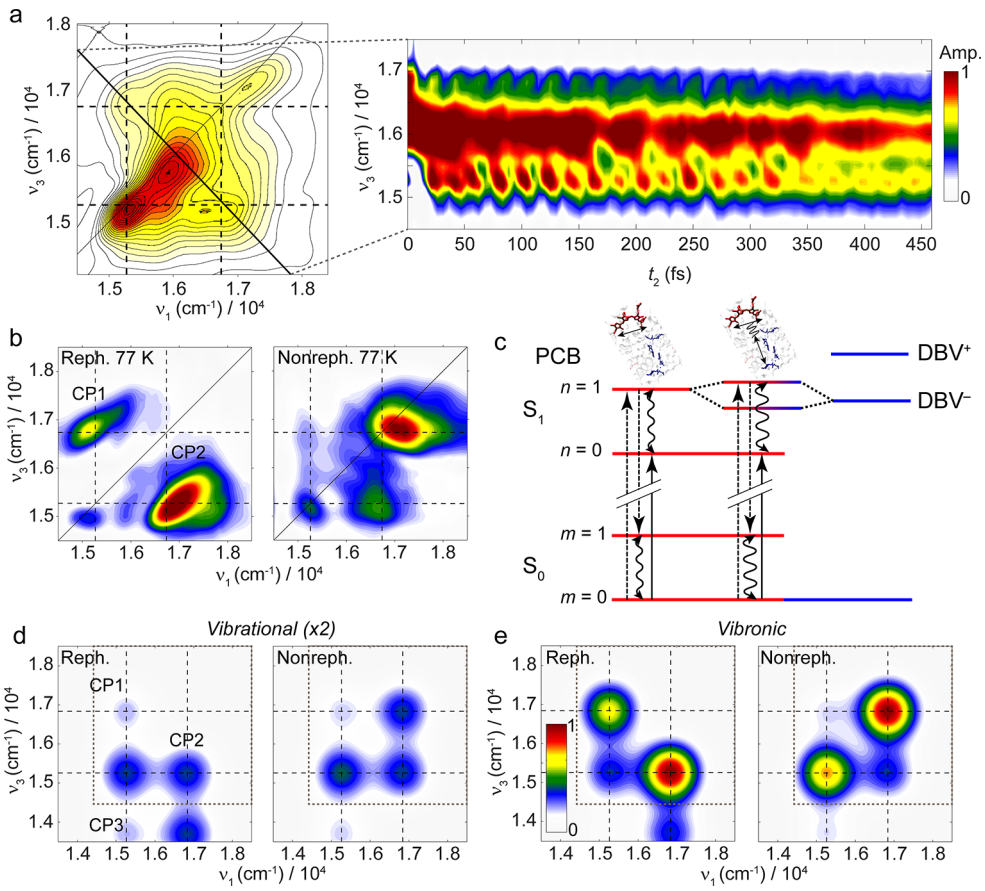

Figure 8. PC645 coherences.[18] (a) Antidiagonal evolution through DBV and PCB cross-peaks at 77 K. (b) Rephasing and non-rephasing coherence maps for $\nu_2 \approx 1600$ cm^{-1} at 77 K. (c) Energy-level diagram depicting the PCB vibrational model (left) and coherences, and (right) the vibronic mixing scenario and coherences incorporated in panel e. (d, e) Simulated coherence maps for (d) PCB vibrational coherence and (e) interpigment vibronic coherence from mixing of PCB (n = 1) and DBV (n = 0). Reprinted with permission from ref 18. Copyright 2016 Elsevier Inc.

excited *and* ground state coherences are enhanced since the ground state excitation is still relayed through an enhanced upper state (resonant excitation).[12] Since CP2 incorporates both a GSB and SE "amplified" signal, it is present at about twice the amplitude of the pure excited state CP1 feature.

These specific signal amplifications, realized through vibronic intensity borrowing, yield a unique set of 2D spectral fingerprints. Cataloguing these salient patterns enables the careful experimentalist to immediately recognize such inter-chromophoric interactions, to which pigments they are active, and the mode(s) facilitating the resonance. Furthermore, these simple amplitude calculations coupled with the vibronic model permits one to relate the coherence spectroscopy back to the wave function picture to evaluate the functional significance of the interactions. For PC645, it was indeed found that the vibronic surface distortions giving rise to the coherence amplitudes also modified the energy transfer mechanism leading to a DBV → PCB rate enhancement of 1.6× the Förster rate.[18] The rate enhancements gained through the vibronic interaction act to direct energy flow, even over large energy gaps separating the chemically different pigments in phycobiliproteins.[31] It is perhaps a key design element in phycobiliproteins for rapid down-conversion, ensuring that the excitation is available for delivery to PSI/PSII prior to quenching processes.

VI. CONCLUSIONS AND OUTLOOK

Coherences have long been utilized as probes of ultrafast dynamics. However, in most cases, understanding their origin is complicated by the various coherent pathways contributing to signal generation in coherent nonlinear experiments. 2D electronic spectroscopy disperses the multitude of coherence signals arising in nonlinear experiments, and this spectral decomposition helps to disentangle coherences of separate origin. In particular, by transforming the coherent 2DES data into its 3D spectral form and selecting 2D slices for individual coherences, an unprecedented level of detail can be realized for the condensed phase and interpreted simply by 2D pattern recognition. Furthermore, the frequency-domain representation of the data can easily be compared against time-independent spectroscopic models that are inherently structure-driven; incorporating molecular parameters that can be determined *ab initio*. Taken together, the joint approach presents a two-dimensional fingerprinting method that can be compared directly against experimental 2D coherence data. Here, several examples were given that embark on building a library of such characteristic fingerprints for ground and excited state vibrational coherences (fundamentals, overtones, and combinations), electronic coherence, and finally mixed electronic–vibrational coherences. Though the time-independent model has its limitations, the simple implementation and direct comparison with calculable molecular parameters makes it a useful protocol for promptly evaluating coherences.

DOI: 10.1021/acs.accounts.7b00369
Acc. Chem. Res. XXXX, XXX, XXX−XXX

AUTHOR INFORMATION

Corresponding Authors

*E-mail: jacobdean@suu.edu.
*E-mail: gscholes@princeton.edu.

ORCID

Gregory D. Scholes: 0000-0003-3336-7960

Funding

This work was supported as part of the Photosynthetic Antenna Research Center, an Energy Frontier Research Center funded by the Basic Energy Sciences program of the US Department of Energy Office of Science under award DE-SC0001035.

Notes

The authors declare no competing financial interest.

Biographies

Jacob C. Dean received his Ph.D. in Chemistry from Purdue University under the advisement of Prof. Tim Zwier. He later became a postdoctoral researcher at the University of Toronto and Princeton University under Prof. Scholes focusing on two-dimensional spectroscopy and coherence analysis of light-harvesting complexes. He is currently an Assistant Professor of Chemistry at Southern Utah University where he is focused on the spectroscopy and photophysics of biomolecules related to photosynthesis.

Gregory D. Scholes is the William S. Tod Professor of Chemistry at Princeton University. Originally from Melbourne, Australia, he later undertook postdoctoral training at Imperial College London and University of California, Berkeley. He started his independent career at the University of Toronto (2000−2014) and is currently the Deputy Editor for the *Journal of Physical Chemistry Letters,* Fellow of the Royal Society of Canada, a Senior Fellow in the Canadian Institute for Advanced Research program *Biology, Energy, Technology*, and a Professorial Fellow at the University of Melbourne. Dr. Scholes has had a long-standing interest in mechanisms of electronic energy transfer and the photophysics of molecular excitons.

REFERENCES

(1) Heller, E. J. The semiclassical way to molecular spectroscopy. *Acc. Chem. Res.* **1981**, *14*, 368−375.
(2) Tannor, D. J. *Introduction to Quantum Mechanics: A Time-Dependent Perspective*; University Science Books, 2007.
(3) Gruebele, M.; Zewail, A. H. Femtosecond Wave Packet Spectroscopy - Coherences, the Potential, and Structural Determination. *J. Chem. Phys.* **1993**, *98*, 883−902.
(4) Pollard, W. T.; Dexheimer, S. L.; Wang, Q.; Peteanu, L. A.; Shank, C. V.; Mathies, R. A. Theory of Dynamic Absorption-Spectroscopy of Nonstationary States 0.4. Application to 12-Fs Resonant Impulsive Raman-Spectroscopy of Bacteriorhodopsin. *J. Phys. Chem.* **1992**, *96*, 6147−6158.
(5) Pollard, W. T.; Lee, S. Y.; Mathies, R. A. Wave Packet Theory of Dynamic Absorption-Spectra in Femtosecond Pump-Probe Experiments. *J. Chem. Phys.* **1990**, *92*, 4012−4029.
(6) Liebel, M.; Schnedermann, C.; Wende, T.; Kukura, P. Principles and Applications of Broadband Impulsive Vibrational Spectroscopy. *J. Phys. Chem. A* **2015**, *119*, 9506−9517.
(7) Cassette, E.; Pensack, R. D.; Mahler, B.; Scholes, G. D. Room-temperature exciton coherence and dephasing in two-dimensional nanostructures. *Nat. Commun.* **2015**, *6*, 6086.
(8) Chenu, A.; Christensson, N.; Kauffmann, H. F.; Mancal, T. Enhancement of Vibronic and Ground-State Vibrational Coherences in 2D Spectra of Photosynthetic Complexes. *Sci. Rep.* **2013**, *3*, 2029.
(9) Christensson, N.; Kauffmann, H. F.; Pullerits, T.; Mancal, T. Origin of Long-Lived Coherences in Light-Harvesting Complexes. *J. Phys. Chem. B* **2012**, *116*, 7449−7454.
(10) Fuller, F. D.; Pan, J.; Gelzinis, A.; Butkus, V.; Senlik, S. S.; Wilcox, D. E.; Yocum, C. F.; Valkunas, L.; Abramavicius, D.; Ogilvie, J. P. Vibronic coherence in oxygenic photosynthesis. *Nat. Chem.* **2014**, *6*, 706−711.
(11) Romero, E.; Augulis, R.; Novoderezhkin, V. I.; Ferretti, M.; Thieme, J.; Zigmantas, D.; van Grondelle, R. Quantum coherence in photosynthesis for efficient solar-energy conversion. *Nat. Phys.* **2014**, *10*, 676−682.
(12) Tiwari, V.; Peters, W. K.; Jonas, D. M. Electronic resonance with anticorrelated pigment vibrations drives photosynthetic energy transfer outside the adiabatic framework. *Proc. Natl. Acad. Sci. U. S. A.* **2013**, *110*, 1203−1208.
(13) Womick, J. M.; West, B.; Scherer, N. F.; Moran, A. M. Vibronic effects in the spectroscopy and dynamics of C-phycocyanin. *J. Phys. B: At., Mol. Opt. Phys.* **2012**, *45*, 154016.
(14) Schlau-Cohen, G. S.; Dawlaty, J. M.; Fleming, G. R. Ultrafast Multidimensional Spectroscopy: Principles and Applications to Photosynthetic Systems. *IEEE J. Sel. Top. Quantum Electron.* **2012**, *18*, 283−295.
(15) Anna, J. M.; Song, Y.; Dinshaw, R.; Scholes, G. D. Two-dimensional electronic spectroscopy for mapping molecular photophysics. *Pure Appl. Chem.* **2013**, *85*, 1307−1319.
(16) Mukamel, S. *Principles of Nonlinear Optical Spectroscopy*; Oxford University Press, 1999.
(17) Egorova, D. Self-Analysis of Coherent Oscillations in Time-Resolved Optical Signals. *J. Phys. Chem. A* **2014**, *118*, 10259−10267.
(18) Dean, J. C.; Mirkovic, T.; Toa, Z. S. D.; Oblinsky, D. G.; Scholes, G. D. Vibronic Enhancement of Algae Light Harvesting. *Chem.* **2016**, *1*, 858−872.
(19) Dean, J. C.; Rafiq, S.; Oblinsky, D. G.; Cassette, E.; Jumper, C. C.; Scholes, G. D. Broadband Transient Absorption and Two-Dimensional Electronic Spectroscopy of Methylene Blue. *J. Phys. Chem. A* **2015**, *119*, 9098−9108.
(20) Chen, J.; Cesario, T. C.; Rentzepis, P. M. Time resolved spectroscopic studies of methylene blue and phenothiazine derivatives used for bacteria inactivation. *Chem. Phys. Lett.* **2010**, *498*, 81−85.
(21) Cina, J. A.; Kovac, P. A.; Jumper, C. C.; Dean, J. C.; Scholes, G. D. Ultrafast transient absorption revisited: Phase-flips, spectral fingers, and other dynamical features. *J. Chem. Phys.* **2016**, *144*, 175102.
(22) Blankenship, R. E. *Molecular Mechanisms of Photosynthesis*; 2nd ed.; Wiley Blackwell, 2014.
(23) Scholes, G. D.; Fleming, G. R.; Olaya-Castro, A.; van Grondelle, R. Lessons from nature about solar light harvesting. *Nat. Chem.* **2011**, *3*, 763−774.
(24) Mirkovic, T.; Ostroumov, E. E.; Anna, J. M.; van Grondelle, R.; Govindjee; Scholes, G. D. Light Absorption and Energy Transfer in the Antenna Complexes of Photosynthetic Organisms. *Chem. Rev.* **2017**, *117*, 249−293.
(25) Laos, A. J.; Dean, J. C.; Toa, Z. S. D.; Wilk, K. E.; Scholes, G. D.; Curmi, P. M. G.; Thordarson, P. Cooperative Subunit Refolding of a Light-Harvesting Protein through a Self-Chaperone Mechanism. *Angew. Chem.* **2017**, *129*, 8504−8508.
(26) Engel, G. S.; Calhoun, T. R.; Read, E. L.; Ahn, T. K.; Mancal, T.; Cheng, Y. C.; Blankenship, R. E.; Fleming, G. R. Evidence for wavelike energy transfer through quantum coherence in photosynthetic systems. *Nature* **2007**, *446*, 782−786.
(27) Collini, E.; Wong, C. Y.; Wilk, K. E.; Curmi, P. M. G.; Brumer, P.; Scholes, G. D. Coherently wired light-harvesting in photosynthetic marine algae at ambient temperature. *Nature* **2010**, *463*, 644−647.
(28) Ferretti, M.; Novoderezhkin, V. I.; Romero, E.; Augulis, R.; Pandit, A.; Zigmantas, D.; van Grondelle, R. The nature of coherences in the B820 bacteriochlorophyll dimer revealed by two-dimensional electronic spectroscopy. *Phys. Chem. Chem. Phys.* **2014**, *16*, 9930−9939.
(29) Lim, J.; Palecek, D.; Caycedo-Soler, F.; Lincoln, C. N.; Prior, J.; von Berlepsch, H.; Huelga, S. F.; Plenio, M. B.; Zigmantas, D.; Hauer, J. Vibronic origin of long-lived coherence in an artificial molecular light harvester. *Nat. Commun.* **2015**, *6*, 7755.

DOI: 10.1021/acs.accounts.7b00369
Acc. Chem. Res. XXXX, XXX, XXX−XXX

(30) Womick, J. M.; Moran, A. M. Vibronic Enhancement of Exciton Sizes and Energy Transport in Photosynthetic Complexes. *J. Phys. Chem. B* **2011**, *115*, 1347−1356.
(31) Kolli, A.; O'Reilly, E. J.; Scholes, G. D.; Olaya-Castro, A. The fundamental role of quantized vibrations in coherent light harvesting by cryptophyte algae. *J. Chem. Phys.* **2012**, *137*, 174109.
(32) O'Reilly, E. J.; Olaya-Castro, A. Non-classicality of the molecular vibrations assisting exciton energy transfer at room temperature. *Nat. Commun.* **2014**, *5*, 3012.
(33) Lee, M. K.; Bravaya, K. B.; Coker, D. F. First-Principles Models for Biological Light-Harvesting: Phycobiliprotein Complexes from Cryptophyte Algae. *J. Am. Chem. Soc.* **2017**, *139*, 7803−7814.
(34) Butkus, V.; Zigmantas, D.; Abramavicius, D.; Valkunas, L. Distinctive character of electronic and vibrational coherences in disordered molecular aggregates. *Chem. Phys. Lett.* **2013**, *587*, 93−98.
(35) Cheng, Y. C.; Fleming, G. R. Coherence quantum beats in two-dimensional electronic spectroscopy. *J. Phys. Chem. A* **2008**, *112*, 4254−4260.
(36) Turner, D. B.; Wilk, K. E.; Curmi, P. M. G.; Scholes, G. D. Comparison of Electronic and Vibrational Coherence Measured by Two-Dimensional Electronic Spectroscopy. *J. Phys. Chem. Lett.* **2011**, *2*, 1904−1911.
(37) Reimers, J. R.; McKemmish, L. K.; McKenzie, R. H.; Hush, N. S. Non-adiabatic effects in thermochemistry, spectroscopy and kinetics: the general importance of all three Born-Oppenheimer breakdown corrections. *Phys. Chem. Chem. Phys.* **2015**, *17*, 24641−24665.

DOI: 10.1021/acs.accounts.7b00369
Acc. Chem. Res. XXXX, XXX, XXX−XXX